

# A Polyethylene-B<sub>4</sub>C based concrete for enhanced neutron shielding at neutron research facilities

D. D. DiJulio<sup>a,b,\*</sup>, C. P. Cooper-Jensen<sup>a,c</sup>, H. Perrey<sup>a,b</sup>, K. Fissum<sup>b</sup>, E. Rofors<sup>b</sup>, J. Scherzinger<sup>b</sup>, P. M. Bentley<sup>a,c</sup>

<sup>a</sup>*European Spallation Source ERIC, P.O. Box 176, SE-221 00 Lund, Sweden*

<sup>b</sup>*Division of Nuclear Physics, Lund University, SE-221 00 Lund, Sweden*

<sup>c</sup>*Department of Physics and Astronomy, Uppsala University, Sweden*

---

## Abstract

We present the development of a specialized concrete for neutron shielding at neutron research facilities, based on the addition of hydrogen atoms in the form of polyethylene and also B<sub>4</sub>C for enhancing the neutron capture properties of the concrete. We show information on the mechanical properties of the concrete and the neutronics, in particular it's relevance to modern spallation neutron sources, such as the European Spallation Source (ESS), currently under construction in Lund, Sweden. The new concrete exhibits a 15% lower mass density, a compressible strength of 50% relative to a standard concrete and a significant increase in performance of shielding against MeV neutrons and lower energies. The concrete could find application at the ESS in for example common shielding components, individual beamline shielding and instrument caves. Initial neutronic tests of the concrete, carried out at Lund University, have also verified the performance in the MeV neutron energy range and the results are presented.

*Keywords:* Neutron shielding, spallation neutron sources, neutron science, Geant4

---

\*Corresponding Author

*Email address:* Douglas.DiJulio@ess.se (D. D. DiJulio)

## 1. Introduction

Neutron research facilities offer scientists the opportunity to use thermal and cold neutrons for scientific investigations in both fundamental and applied sciences. At spallation neutron sources, such as the European Spallation Source (ESS) [1], currently under construction in Lund, Sweden, the creation of these cold and thermal neutrons involves the bombardment of a heavy metal target with an intense and high-energy proton beam. The neutrons that escape the target can undergo scattering in moderators placed in the vicinity of the target and are ultimately guided towards the sample position of a neutron instrument, which can be up to around a couple of hundred meters away from the target. However, the neutrons that are not slowed down, in addition to other high-energy particles, can travel deep into the shielding, which surrounds the target and moderators, and induce the creation of secondary particles that could also reach the location of a neutron instrument. These unwanted particles are time-correlated with the proton beam pulse and may lead to backgrounds which make measuring weak signals impossible or challenging [2]. Therefore, neutron shielding not only plays an important role for radiation safety purposes, but also for minimizing the unwanted background noise in neutron instruments.

The bulk shielding at spallation neutron sources typically consists of steel and concrete. The choice of these materials is due to a number of different reasons. The attenuation of high-energy neutrons, above 10s of MeVs, is primarily through nuclear reactions and also at high-energies the attenuation lengths are driven by the material density, and therefore materials which are based on metals perform effectively. Below this energy range, hydrogen containing materials are well suited for the slowing down of neutrons. Compared to iron, which requires 410 collisions to slow a neutron down from 2 MeV to 1 eV, only 15 collisions are required for hydrogen [3]. Thus hydrogen containing materials such as concrete can be used to effectively reduce the energy of incident neutrons, especially around a few MeV and lower, to a regime where the absorption cross-section is larger for most materials. Furthermore, in this energy range,

metal-based materials exhibit a significant number of pronounced minima in their cross-sections, called windows. Any neutron which is scattered into one of these windows will have a long mean-free path in the material and can travel a long distance. The addition of concrete shielding thus also serves the role of blocking the windows in the metal-based shielding. The concrete shielding can also often contain boron for instance, as in the outer layers of the shielding monolith at the Swiss Spallation Neutron Source (SINQ [4]) at the Paul Scherrer Institute, Villigen, Switzerland, in order to absorb the neutrons which have slowed down to thermal energies. The final selection of the shielding materials is then a trade-off between these physics properties and for example the cost of the materials, floor loading and operational requirements, just to name a few.

Both experimental and theoretical evidence for the features described above have been observed in for example earlier studies at the ISIS spallation neutron source [5] at the Rutherford Appleton Laboratory [6]. Simulations and measurements revealed that the penetration energy spectra of neutrons through bulk shielding, consisting of iron and concrete, have a broad component which peaks between  $10^{-4}$  and 10 MeV, corresponding to the slowing down of neutrons in concrete and iron shielding [7, 8]. Additionally, a recent survey carried out at the Spallation Neutron Source (SNS), Oakridge, Tennessee, USA [9] also suggested that the dominant component of neutron leakage through the bulk shielding around the target was likely related to neutrons on the order of a few MeVs [10]. Therefore, continued research and development into new shielding solutions could be considered of great interest to both current modern and future spallation neutron sources. An example of a recent development within this field can be found in [11], where the authors presented a steel resin, paraffin/polyethylene (PE) and boron mixture as a possible replacement for heavy concrete at a neutron research facility.

For the above mentioned reasons, we investigated and developed a new specialized concrete for enhanced neutron shielding. The new design was based on increasing the hydrogen content in concrete with the final aim of an improved minimization of neutrons in the MeV and lower energy ranges and with the goal

of increasing neutron instrument performance at spallation neutron sources. In the following, we present a description of the concrete, including its neutronic and mechanical properties, followed by an experimental verification of the concrete in the MeV neutron range.

## 2. Design of the Concrete

### 2.1. Performance at a spallation neutron source

The main motivation behind the concrete was to increase the concentration of hydrogen through the addition of PE, in addition to boron in the form of  $B_4C$ . Early studies of adding hydrogen to concrete, in the form of water, found that a 7 wt% water content was sufficient for the slowing down of intermediate-energy neutrons to the thermal energy range at a nuclear reactor [12]. It was also concluded that a greater water content would only improve the neutron attenuation properties of the concrete. The idea of adding boron to concrete is also well known, where early efforts were aimed at reducing the dose behind a neutron shield due to neutron capture photons through the addition of boron. A detailed early overview can be found in [13]. The neutronic benefits of adding the combination of both hydrogen in the form of PE and  $B_4C$  to concrete has also been studied in detail previously in a more recent publication [14], however no results on the actual construction or neutronic testing of the proposed PE- $B_4C$ -based concrete were presented.

To investigate the potential for using such a concrete at a spallation neutron source, we carried out simulations of the performance of the concrete over the entire relevant energy range. For these purposes, we used an incident energy spectrum from a Geant4 [15, 16] model based on the technical-design-report concept of the ESS [17]. This spectrum represents the total number of neutrons over four  $60^\circ$  beamline extraction areas, at 2 m from the moderator position. This spectrum was then used as input to simulations and incident on various concrete blocks, of different compositions, and with a thickness of 25 cm. Each block was infinite in dimensions in the lateral directions and was followed by

a detector of the same lateral dimensions, placed directly behind the position of a block. While the concrete is not planned to be used as a beamstop, these simulations illustrate the effects of modifying the composition of concrete over a wide energy range. The calculations were also carried out using Geant4 and the composition of the two concretes which were investigated are given in Table 1, which is based on the mixing recipe presented in the next section. The physics list QGSP\_BERT\_HP [18] was used for the simulations.

The results of the simulations are shown in Fig. 1. The green curve indicates the incident ESS beam and the other curves show the transmission of this beam through the indicated material compositions and thicknesses. The standard reference concrete is indicated by the red line, where one can see the thermal peak at low energies. The purple curve shows the result of adding 10% by weight of PE to the reference concrete, where it can be seen that while the thermal peak still remains, the region between 1 eV and 1 MeV is greatly reduced. If only B<sub>4</sub>C is added to the reference concrete (blue curve), the thermal peak is removed but little effect is seen between 1 eV and 1 MeV. The black curve represents the addition of both the PE and B<sub>4</sub>C (referred to as PE-B<sub>4</sub>C-concrete), where the combined effect of these two components is clearly seen in the new concrete. Our calculations also showed that in order to reach the same level of performance for 1 eV to 1 MeV neutrons as PE-B<sub>4</sub>C-concrete, 60% more reference concrete or B<sub>4</sub>C-only concrete would be needed. This illustrates one of the major benefits of such a concrete, that it would be both lighter and less material would be needed in order to match the performance of thicker blocks of more standard types of concretes.

We also investigated the simulated prompt-photon production due to neutron interactions in the different concrete material compositions, and the results are shown in Fig. 2. The simulation conditions were the same as described above. The addition of the PE to the concrete had little effect on the photon production and thus the figure only presents results for the reference concrete and the PE-B<sub>4</sub>C-concrete. The addition of the B<sub>4</sub>C resulted in approximately a third of the photon production compared to the standard concrete. Above 0.5

MeV, this reduction was closer to an order of magnitude. These results indicate that such a concrete can also be used to lower the radiation dose due to photons outside of a thick shield, as discussed earlier.

It can be mentioned that these calculations assume that the PE and B<sub>4</sub>C are homogeneously distributed throughout the concrete block. The effects of inhomogeneities and grain sizes of the additives, for example as seen in previous studies of Boral are not considered [19, 20].

## *2.2. Construction of the concrete*

Inspired by the above presented simulations, we had a concrete mixture produced based on the addition of PE and B<sub>4</sub>C. The recipe for the concrete is shown in Table 2, for both the reference concrete and the new concrete. The mixing of the concrete was performed by the Danish Technological Institute (DTI) [21, 22] and it was found that a 50-50 mix by weight of 2.5 mm and 5.0 mm PE beads provided a homogeneous mixture of the PE throughout the concrete. The indicated dimensions correspond to both the length and diameter of a tube of PE. As can be seen in the table, the PE replaced a fraction of the granite, ultimately giving 10% by weight PE for the PE-B<sub>4</sub>C-concrete. The combined volume of the granite and PE in the PE-B<sub>4</sub>C-concrete was equal to the volume of the granite in the reference concrete. A total of 0.76 wt% B<sub>4</sub>C was added to the concrete, and it replaced some of the sand as both have similar grain size and mass density. The grain size of the B<sub>4</sub>C was smaller than 1 mm. A picture of the produced concrete is shown Fig. 3, where the B<sub>4</sub>C is not visible but the white spots are the PE beads dispersed in the concrete. The larger black and pink spots are the granite. The total weight fraction of water in the concrete was around 8%.

Fig. 4 shows a comparison of the compressive strength of the two concretes after 7 days, 28 days and 56 days. As some of the granite was replaced by PE, it can be expected that the strength of PE-B<sub>4</sub>C-concrete is lower than that of the standard concrete. After 28 days, the concretes have obtained the majority of their strength, but over time they will still get a little stronger.

Fig. 5 shows the mass densities of the concretes at different locations along a single meter long column. As one can see from the figure, PE-B4C-concrete also has a lower density than the standard concrete. This is also due to the replacement of the granite, with a mass density of about  $2.6 \text{ g/cm}^3$  with the PE, which has a density of  $0.95 \text{ g/cm}^3$ . The lower density of the new concrete thus corresponds to a concrete that is overall 15% lighter than regular concrete. The figure also illustrates the homogeneity of the mass density of the PE-B4C-concrete throughout the column.

### 3. MeV neutron measurements

In order to evaluate the performance of the concrete, in the MeV range, we carried out shielding measurements using the time-of-flight (TOF) technique. The aim of the current measurements was to verify the general neutronic behavior of the concrete in the MeV neutron energy range, and a detailed discussion of the experimental setup and technique will be the highlight of a future publication [23]. However, a general overview of the setup is given below.

The measurements were carried out using the method of neutron tagging [24] at the Source-Testing Facility at the Division of Nuclear Physics at Lund University with neutron energies between 1-7 MeV. Neutron tagging involves measuring the TOF (and thus energy) of individual neutrons emitted from a radioactive source on an event-by-event basis. For the measurements reported here, a  $^{238}\text{Pu}/^9\text{Be}$  source was employed. Fast neutrons are produced during a two-step process. The actinide  $^{238}\text{Pu}$  first decays by emitting  $\alpha$  particles with a mean energy of 5.4891 MeV [25]. If the  $\alpha$ -particle reacts with  $^9\text{Be}$ , neutrons with energies up to about 11 MeV could be freed [26]. The Pu/Be source radiated approximately  $2.99 \times 10^6$  neutrons per second [27]. For further details about the source, see Ref. [28].

In the special case that the  $^{12}\text{C}$  nucleus recoils in its first-excited state, the neutron will be accompanied by a prompt 4.44 MeV de-excitation  $\gamma$ -ray radiated almost isotropically. The resulting radiation field of interest when this occurs is

thus a combination of 4.44 MeV  $\gamma$ -rays and their associated neutrons. Detection of the 4.44 MeV  $\gamma$ -ray allows for the determination of the instant in time when the corresponding neutron was emitted from the source. Detection of the corresponding neutron, a tagged-neutron event, then allows for the determination of the neutron TOF. The detection of two simultaneous  $\gamma$ -rays from the source was used for calibration of the TOF measurement, as described in [29]. Note that the tagging technique restricts the maximum available tagged-neutron energies to about 7 MeV due to the energy lost to the 4.44 MeV  $\gamma$ -ray.

For the measurements, the neutron source was located at the center of a water tank with open tangential beam ports. The blocks of materials were placed approximately one meter from the position of the source, and an NE-213 detector was located directly behind the blocks. This detector provided a start signal for the data acquisition and the delayed stop signal was provided by YAP detectors which were triggered off the 4.44 MeV photons emitted from the source. The size of the neutron beam on the samples ranged from about 12 cm to 14 cm, which depended on the sample to detector distance which was used for the measurements. Additionally, no pulse-shape discrimination was applied in the analysis, as the events which fall within the TOF range of interest are comprised primarily of neutron events [28].

The measured direct TOF spectrum is shown in Fig. 6 in the left panel and the spectrum converted to energy in the right panel. Multiple scattering effects with the water walls of the tank were not included in this conversion. For the shielding measurements, four materials were used as benchmarks for simulations. These included blocks of steel, copper and PE in addition to the reference concrete. For the steel, copper, and PE measurements, the total material thickness corresponded to 20 cm. The width and height of the blocks were 20 cm. For both concrete samples, the total thickness was 25.5 cm with a width and height of 25.5 cm.

A model of the above described setup was implemented in Geant4. This included the direct beam, as shown in Fig. 6, the divergence of the beam provided by the tank, the distances between the source and detectors, the thicknesses of

the blocks, and the detector efficiency, as modeled with the Stanton code [30]. A lower energy cutoff of 300 keVee was used during the analysis, which resulted in a lower energy neutron cutoff of 1 MeV for the neutron detection efficiency. The physics list QGSP\_BERT\_HP was also used for these simulations and the materials compositions for the concretes are those given in Table 1. For the comparison of the measurements to simulations, we used directly the TOF instead of the conversion to energy space, as the conversion would require a detailed knowledge of the multiple-scattering effects within the blocks.

The results with the four benchmark materials are shown in Fig. 7. Overall it is seen that there is excellent agreement between the Geant4 simulations and the measurements. This provides confidence that the simulation method and approximations used are sufficient for predicting the general performance of the blocks for neutron shielding.

Fig. 8 presents a comparison of the measured reference concrete data, the PE-B4C-concrete data, and the simulations, albeit at a slightly different measurement location than those shown in Fig. 7. Again excellent agreement between the simulations and measurements can be seen. The simulations suggest that over the indicated energy range, there is roughly 40% fewer neutrons entering the detector for the PE-B4C-concrete relative to the reference concrete.

#### 4. Conclusions

In summary, we have developed a specialized concrete for enhanced suppression of neutrons below the few MeV energy range. The concrete was created by adding PE beads and  $B_4C$  to the material mixture. We found that while the concrete was not as strong as the reference concrete, it exhibited a lower density and a significant improvement in the shielding of neutrons below a few MeVs compared to the standard concrete. An analysis of our measurement data revealed that the new concrete yields around 40% fewer neutrons, compared to a standard concrete, in the MeV energy range while Fig. 1 suggests that the improvements are roughly a factor of 10 in the eV-keV range and even better at

lower energies. It is anticipated that the new concrete could find application in either bulk shielding at spallation neutron sources and/or in specific beamline components such as beamline shielding or instrument caves. It should also be mentioned that the concrete could find applications at reactor- and/or other accelerator-based neutron research facilities.

## 5. Acknowledgments

This project has received funding from the European Unions Horizon 2020 research and innovation programme under grant agreement No 654000.

## References

- [1] S. Peggs, et al., ESS Technical Design Report, Lund, Sweden, 2013.
- [2] N. Cherkashyna, et al., Proceedings of ICANS XXI (International Collaboration on Advanced Neutron Sources) JAEA-Conf 2015-002 (2015) 479.
- [3] G. Bauer, Nucl. Instr. and Meth. in Phys. Res. A 463 (2001) 505.
- [4] SING - The Swiss Spallation Neutron Source, <https://www.psi.ch/sinq/>.
- [5] ISIS - ISIS Home Page, <http://www.isis.stfc.ac.uk/>.
- [6] Rutherford Appleton Laboratory - Science and Technology Facilities Council, <http://www.stfc.ac.uk/about-us/where-we-work/rutherford-appleton-laboratory/>.
- [7] T. Nunomiya, et al., Nucl. Instr. and Meth. in Phys. Res. B 179 (2001) 89.
- [8] N. Nakao, et al., Nucl. Instr. and Meth. in Phys. Res. A 530 (2004) 379.
- [9] Spallation Neutron Source, <https://neutrons.ornl.gov/sns>.
- [10] D.D.DiJulio, et al., J. Phys. Conf. Ser. 746 (2016) 012033.
- [11] E. Calzada, et al., Nucl. Instr. and Meth. Phys. Res. A 651 (2011) 77.

- [12] E.P.Blizard, J. M.Miller, Radiation Attenuation Characteristics Of Structural Concrete, Oak Ridge National Laboratory, 1958.
- [13] F. A. R.Schmidt, The Attenuation Properties Of Concrete For Shielding Of Neutrons Of Energy Less Than 15 MeV, Oak Ridge National Laboratory, 1970.
- [14] S. Park, et al., J. Nucl. Materials 452 (2014) 205.
- [15] Geant4, <http://www.geant4.org>.
- [16] S. Agostinelli, et al., Nucl. Instr. Meth. A 506 (2003) 250.
- [17] D.D.DiJulio, et al., J. Phys. Conf. Ser. 746 (2016) 012032.
- [18] Geant4 Physics Lists, <http://geant4.cern.ch/support>.
- [19] W. Burrus, Radiation transmission through boral and similar heterogeneous materials consisting of randomly distributed absorbing chunks, Oak Ridge National Laboratory, 1960.
- [20] F. Åkerhielm, Transmission of Thermal Neutrons through boral, Aktiebolaget Atomenergi, Stockholm, Sweden, 1960.
- [21] Danish Technological Institute, <http://www.dti.dk/>.
- [22] T. Svensson, C. Pade, Neutron Shielding Concrete - Development of mix design and documentation of selected properties, Danish Technological Institute, 2016.
- [23] H. Perrey, Manuscript in Preparation.
- [24] J. Scherzinger, et al., Appl. Rad. and Isotopes 98 (2015) 74.
- [25] <http://www.nndc.bnl.gov/nudat2/>.
- [26] E. Lorch, J. Appl. Radiat. Isot. 24 (1973) 585.
- [27] Exactly  $4.26 \times 10^6$  neutrons per second. Calibration certified at The Radiochemical Centre, Amersham, England HP7 9LL on 3 September, 1973.

- [28] J. Scherzinger, et al., Manuscript submitted to Appl. Rad. and Isotopes (2016) Preprint available <https://arxiv.org/abs/1611.00213>.
- [29] J. Scherzinger, Neutron Irradiation Techniques, PhD Thesis, Lund University, 2016.
- [30] N. R. Stanton, <https://ntrl.ntis.gov/ntrl/dashboard/searchresults/titledetail/coo154592.xhtml>.

Table 1: Material properties (weight percent and density) for the two concretes used in the simulations.

	Reference Concrete	PE-B4C-concrete
O	51.04%	46.06%
Ca	7.08%	8.05%
Si	32.50%	28.4%
Al	3.68%	2.34%
Fe	1.15%	0.837%
Mg	0.235%	0.195%
Na	1.05%	0.613%
K	2.11%	1.25%
S	0.235%	0.276%
Cl	0.00301%	0.00353%
H	0.782%	2.362%
Ti	0.0903%	0.0517%
P	0.04520%	0.0259%
C		8.93%
B		0.596%
Density	2.34 (g/cm <sup>3</sup> )	1.97 (g/cm <sup>3</sup> )

Table 2: The ingredients used to create 1 m<sup>3</sup> of each of the concretes [22]

Materials	Reference Concrete (kg)	PE-B4C-concrete (kg)
Cement	350.9	347.9
Water	155.7	154.0
Admixture	2.6	2.6
Sand	797.6	765.4
Granite 4/8	258.9	
Granite 8/16	795.3	509.6
PE 2.5 mm		100.1
PE 5.0 mm		101.6
B <sub>4</sub> C		15.0

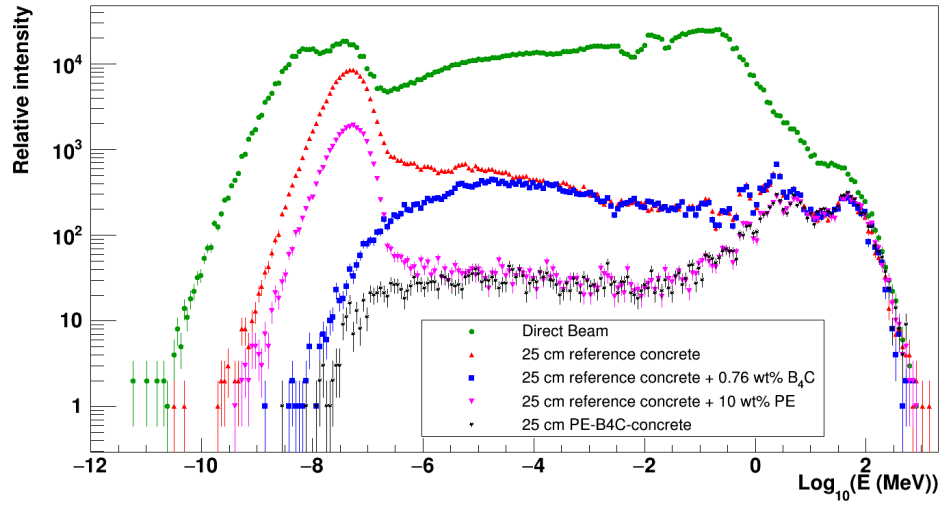


Figure 1: Predictions of the different concrete compositions simulated using Geant4. The green curve is the incident neutron beam with the remaining curves showing the transmission spectra for the indicated material compositions.

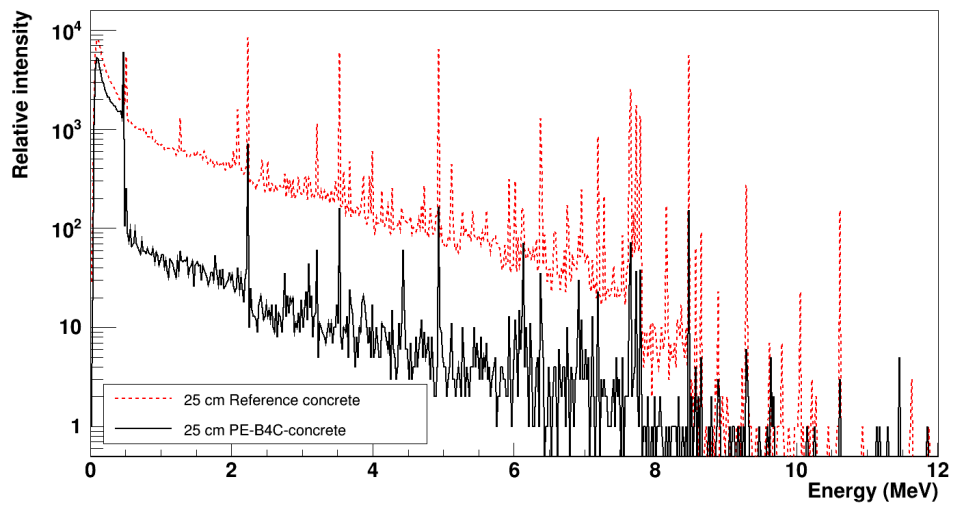


Figure 2: Geant4 predictions of the prompt-photon emission of the reference concrete and the PE-B4C-concrete.



Figure 3: Photo of a cross-section of PE-B4C-concrete, the marker is shown for reference.

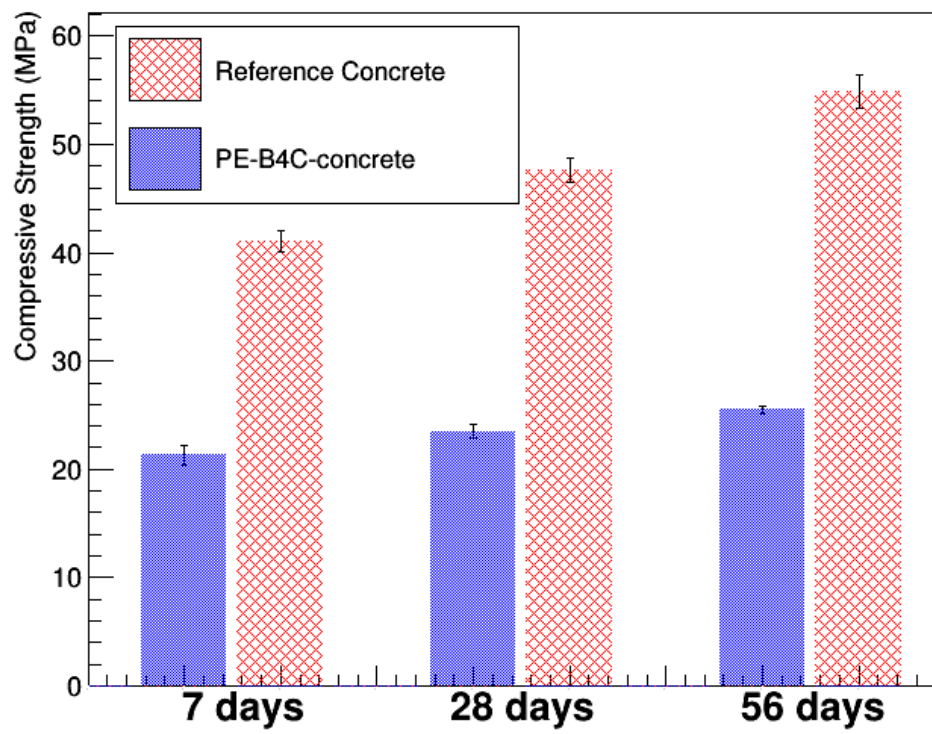


Figure 4: The compressive strength of the reference concrete and PE-B4C-concrete after 7, 28 and 56 days [22].

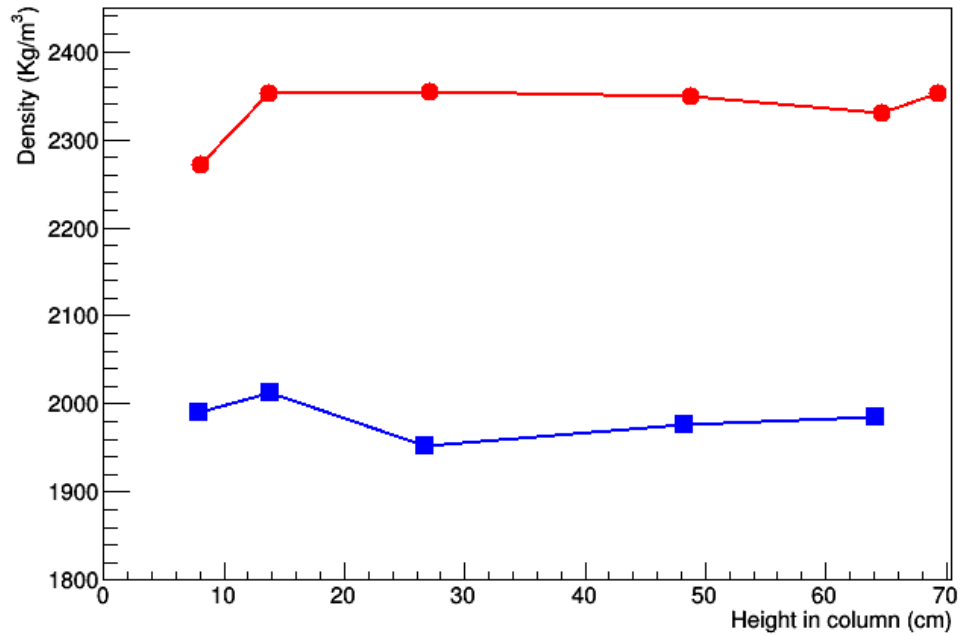


Figure 5: The mass density of the reference concrete and PE-B4C-concrete at different locations throughout a column of the indicated concrete [22].

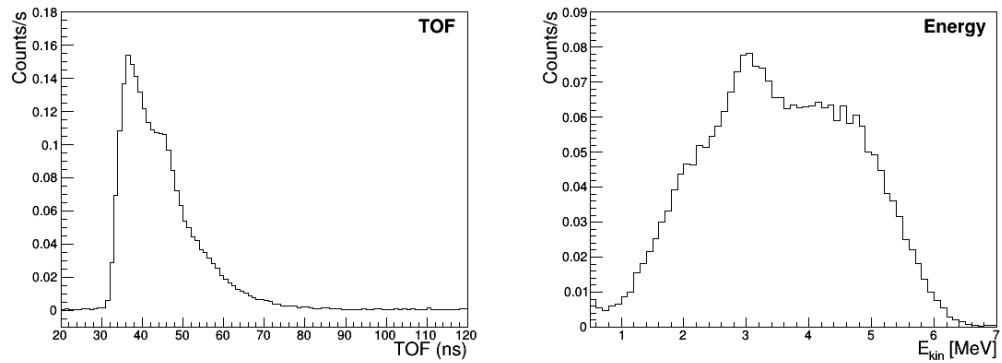


Figure 6: The left panel shows the detected neutron TOF spectrum without any shielding blocks in the beam path. The right panel shows the spectrum converted to energy space, as described in the text.

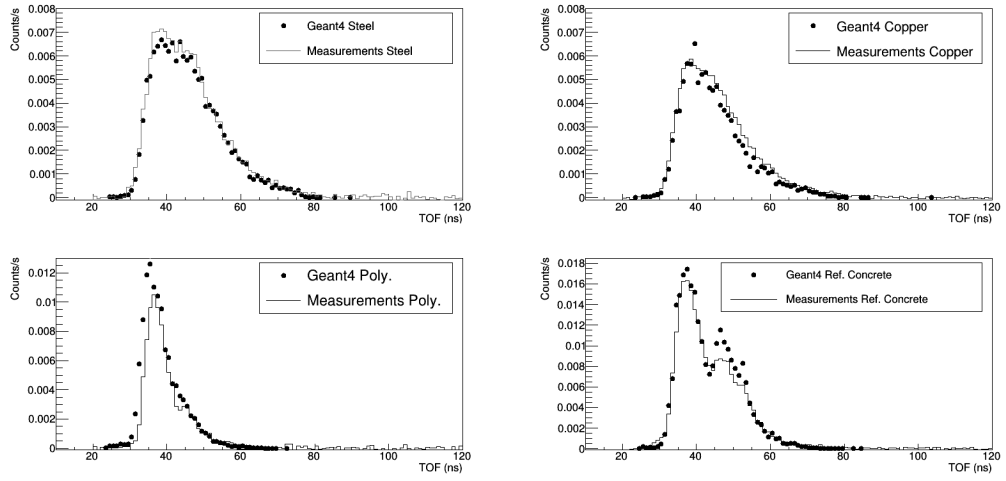


Figure 7: A comparison of measurements and simulations for the four benchmark materials.

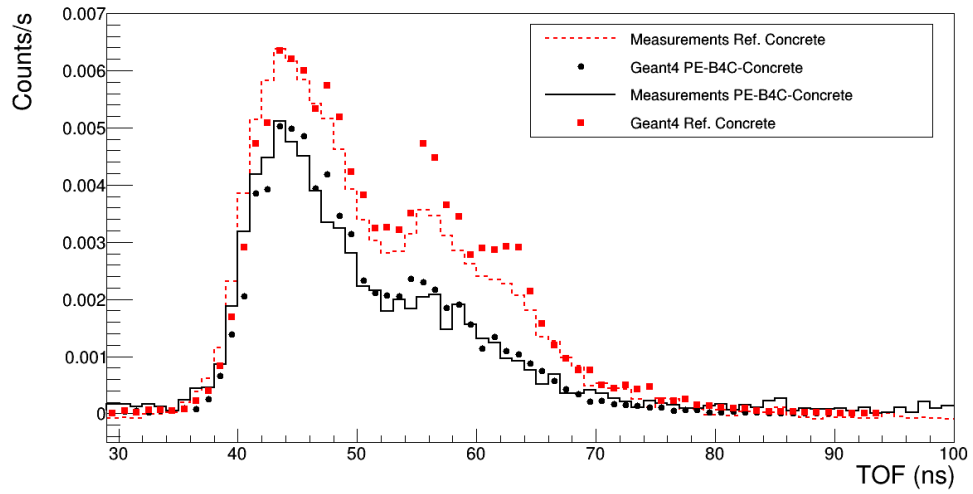


Figure 8: A comparison of measurements and simulations for the reference concrete and PE-B4C-concrete.